Arabian Journal of Chemistry (2022) **15**, 104375

King Saud University

Arabian Journal of Chemistry

www.ksu.edu.sa
www.sciencedirect.com

ORIGINAL ARTICLE

Efficient electrochemical detection of dopamine with carbon nanocoils and copper tetra(p-methoxyphenyl)porphyrin nanocomposite

Syeda Aqsa Batool Bukhari [a], Habib Nasir [a,*], Effat Sitara [a], Tehmina Akhtar [a], Muhammed Ramazan Oduncu [b], Sadia Iram [a], Lujun Pan [c]

[a] *Department of Chemistry, School of Natural Sciences, National University of Sciences and Technology, H-12 Islamabad (44000), Pakistan*
[b] *School of Materials Engineering Neil Armstrong Hall of Engineering 701 West Stadium Avenue, Purdue University, West Lafayette, IN 47907-2045, USA*
[c] *School of Physics and Optoelectronic Technology, Dalian University of Technology, No. 2 Linggong Road, Ganjingzi District, Dalian 116024, PR China*

Received 11 August 2022; accepted 16 October 2022
Available online 20 October 2022

KEYWORDS

Carbon nanocoils;
Dopamine;
Neurotransmitter;
Copper tetra(p-methoxyphenyl)porphyrin;
Electrochemical sensor

Abstract Dopamine (DA), a critical catecholamine neurotransmitter, is responsible for normal functioning of body. Its dysregulation causes cognitive disturbances. Thus, an efficient real time monitoring of DA in clinical samples is required. Herein we report a novel nanocomposite comprising of carbon nanocoils (CNC) and copper tetra(p-methoxyphenyl)porphyrin (CuTMePP) for efficient electrochemical detection of dopamine that was characterized by FTIR, UV/vis., Raman, XRD, SEM, TEM and energy dispersive X-ray techniques. The electrochemical studies were performed using cyclic voltammetry (CV), electrochemical impedance spectroscopy and differential pulse voltammetry (DPV). CNC/CuTMePP/glassy carbon (GC) has demonstrated two linear trends between current and concentration i.e. 0.1 to 100.0 μM and 100.0 to 800.0 μM. Limit of detection (LoD), limit of quantification (LoQ) and sensitivity of the electrode in the concentration range of 0.1 to 100.0 μM was 50.0 nM, 167.0 nM and 1.76 $\mu A \mu M^{-1} cm^{-2}$, respectively using CV. With DPV, the LoD, LoQ and sensitivity were found to be 64.0 nM, 211.0 nM and 0.75 $\mu A \mu M^{-1} cm^{-2}$, respectively obtained in a concentration range of 0.1 to 100.0 μM. The as prepared sensor exhibited good intra/inter-day stabilities, reproducibility, excellent recovery in the human serum samples, presented

* Corresponding author.
E-mail address: habibnasir@sns.nust.edu.pk (H. Nasir).
Peer review under responsibility of King Saud University.

Production and hosting by Elsevier

https://doi.org/10.1016/j.arabjc.2022.104375

significant clinical dopamine detection and showed comparable results with other work in literature.

1. Introduction

Neurotransmitters are endogenous molecules that spontaneously transmit sensory messages from a neuron via synapse to act on a target cell, thus play an important role in the normal brain functioning (Lakard et al., 2021). Dopamine (DA) (3,4-dihydroxyphenethylamine), discovered by Arvid Carlsson in 1957, belongs to the class of biogenic amines of human neurotransmitters (Anuar et al., 2020). This is one of the most important catecholamine neuromodulators responsible for regulation of physiological functions of the body including central nervous, hormonal, renal, emotions and cardiovascular systems (Stoikov et al., 2011; Tavakolian-Ardakani et al., 2019). Abnormal concentration of dopamine can lead to neurodegenerative and physical stress diseases such as Alzheimer (Nam et al., 2018), Parkinson's disease (Latif et al., 2021), and attention-deficit hyperactivity disorder (ADHD) (Pandikumar et al., 2014). Therefore, sensitive, selective and real time detection of DA is of great clinical significance.

Various analytical techniques are being used to detect dopamine (Farajikhah et al., 2019) which include high performance liquid chromatography (HPLC) (Zhao et al., 2011; Chen et al., 2021), chemiluminescence spectroscopy (Palakollu et al., 2020) and electroanalytical detection (Foroughi et al., 2015; Juska and Juska, 2021; Lakard et al., 2021; Li et al., 2021). However, these methods exhibit certain limitations and advantages. Despite the fact that HPLC offers high sensitivity, and selectivity it demands time consuming preliminary treatment of analyte prior to use, which is not suitable for the prompt clinical determination (Foroughi et al., 2021a, 2021b). Similarly, the low sensitivity and instability limits the application of fluorescence spectroscopy for the realistic clinical monitoring. Therefore, the above mentioned analytical techniques mentioned are not suitable for the rapid detection of DA in clinical blood serum samples. Electrochemical analysis has the distinct advantage, such as good specificity, high sensitivity and no intricate prerequisite treatments to monitor DA (Baytak and Aslanoglu, 2020; Fathi et al., 2020). Another advantage of using the electrochemical techniques like voltammetric analysis is the convenient on-site analysis can be performed (Jandaghi et al., 2020).

Based on the superior geometrical and chemical properties, the carbon nanomaterials (like graphene, reduced graphene oxidize, and carbon nanotubes), have become essential tools in the development of electrochemical sensors (Foroughi et al., 2021a, 2021b; Kumar and Srivastva, 2021). Their fascinating properties such as intrinsic electrocatalytic activity, enhanced conductivity, chemical stability, biocompatibility, and large surface area allow them to be used in the field of electrochemical sensors. Supramolecular assemblies of carbon nanomaterials with other suitable receptor molecules increase the sensitivity and selectivity of the sensor for a certain analyte (Zhu, 2017).

Recently, for electrochemical sensing of DA various combinations of reduced graphene oxide and carbon nanotubes with metal oxide nanoparticles (Wu et al., 2012; Bhakta et al., 2015), noble metal nanoparticles (Dursun and Gelmez, 2010; Poudyal et al., 2019), nanoalloys (Yan et al., 2013; Li et al., 2017), metal organic frameworks (Huang et al., 2021), metallated/non-metallated tetraphenylporphyrins (Wu et al., 2012), and phthalocyanines (Pakapongpan et al., 2014; Luhana et al., 2022) etc. have been used. Even though the composites of copper tetraphenylporphyrins with graphene e.g. copper tetraphenylporphyrin/chemically reduced graphene oxide/GCE (Karuppiah et al., 2016) and reduced graphene oxide/tetrakis-(ethoxy carbonyl) porphyrin copper (II) supported glassy carbon electrode (Huang et al., 2018) have been used previously for the detection of dopamine, carbon nanocoils have never been used in such combinations with copper tetraphenylporphyrin derivatives. So, in order to explore a new combination, we used carbon nanocoils (CNC) with copper 5,10,15,20-tetrakis(4-methoxyphenyl) porphyrin (CuTMePP). CNC/CuTMePP exhibited significant performance in terms of limit of detection and stability studies. CNC/CuTMePP/CNC showed excellent electrocatalytic activity in a wider range of concentrations as compared to the earlier reported electrodes. The obtained results revealed that CNC in combination with CuTMePP as receptor could be used to detect DA through electrochemical methods in real time.

Tetraphenylporphyrin and its derivatives can mimic the role of the naturally occurring metallo-porphyrins present in the biological systems (Auwärter et al., 2015). Tetraphenylporphyrins are potent tetradentate ligands as they can easily accommodate different transition and non-transition metal ions (Cu, Zn, Ni, Co, Cd, Pd, Mg, etc). Tetraphenylporphyrin and derivatives have wide range of applications in pigment industry, catalysis, photodynamic therapy, sensors and medicine (Senge et al., 2021). Different protocols are available to synthesize substituted and unsubstituted tetraphenylporphyrins like Rothemund, Adler Longo and Lindsey method, etc. (Efimov and Laaksonen, 2022). In the present work Adler Longo method was used to synthesize tetramethoxyphenyl porphyrin.

Carbon nanocoils are the three-dimensional nanomaterials with solenoid coiled morphology that were discovered by Davis et al. in 1953 (Davis et al., 1953). CNC have been synthesized using different techniques that include thermal chemical vapour deposition (Cui et al., 2014), atomic layer deposition method (Vickers, 2017) and hydrothermal method (Su et al., 2015) using combination of metal oxides as catalyst for growth of nanocoils. The intrinsic properties of carbon nanocoils like mechanical strength, thermal stability, high chemical inertness, immense surface area, outstanding electron transfer capabilities, and low resistance have led to their use as excellent support to immobilize various receptors (Kausar, 2021). Further, carbon nanocoils as such and in the form composites have been explored in the different research fields that includes energy applications (Reddy et al., 2011) viz fuel cells, supercapacitors (Su et al., 2015; Lin and Du, 2021), microwave absorption, and sensors (Zaeri and Ziaei-Rad, 2015; Wu et al., 2019) etc.

In this work, we have constructed a novel nanosensor using carbon nanocoils and copper tetramethoxyphenyl porphyrin for the detection of dopamine. Our nanosensor (CNC/CuTMePP/GC) shows better sensitivity and selectivity for DA as compared to other reported electrodes. Efficient clinical performance of the as prepared nanosensor is comparable to the previously reported work.

2. Experimental

2.1. Chemical reagents

The chemicals utilized in this project include dopamine hydrochloride (98 %), copper (II) acetate monohydrate (≥98 %), N,*N*-dimethyl formamide (99.5 %), and copper acetate were purchased from Sigma Aldrich. Hydrochloric acid (37 %), chloroform (analytical grade Emsure grade), 4-methoxybenzaldehyde, potassium chloride (99.9 %), potassium ferricyanide (≥99 %), potassium dihydrogen phosphate (≥99.5 %), anhydrous dipotassium hydrogen phosphate (Emsure grade for analysis), glucose, sodium chloride (99.5 %), sodium hydroxide pellets (99 %), calcium chloride

dehydrated (Emsure grade) and silica gel (chromatography grade) were procured from Merck. Propionic acid (99 %) from Acros Organics, absolute ethyl alcohol (99.9 %) and acetone (analytical grade) were obtained from Labscan and pyrrole (96 %) from Fluka. Gamma alumina polish (0.05 μm) and diamond polish with particles size equal to 1 μm along with polishing pad and the mounting glass were acquired from Gamry Instruments. De-ionized water (DI water) was used for the preparation of all aqueous solutions. Carbon nanocoils with an average line diameter of 220 nm and a coil pitch of 500 nm were received from Dalian University of Technology (China).

2.2. Instrumentation

2.2.1. Physicochemical analysis

UV–visible spectroscopic analysis of the materials was performed with PerkinElmer spectrometer (Model: Lambda-365) in the region of 300 to 700 nm. For FTIR analysis, attenuated total reflect Fourier transform infrared spectrometer (Bruker, Alpha Platinum, Germany) was used in the range of 550–4000 cm^{-1}. For the study of morphology of the nanocomposites, scanning electron microscope (SEM) (Jeol, JSM-6490A, Japan) was used and energy dispersive X-ray spectroscopy (EDS) was employed to analyze the elemental composition of the materials. Tecnai T20 (FEI) was used to acquire transmission electron microscopic (TEM) images operated at 200 kV with a Gatan US1000 charge-coupled device camera. For XRD analysis, Bruker D8 Advance, Germany XRD Diffractometer with Cu K Alpha X-ray source was used. Analysis was carried out in 2θ range of 5-80°. Raman analysis was carried on i-Raman High Resolution TE Cooled Fiber Optic Raman System (Model: 1064 nm fiber optics, USA) at a wavelength of 532 nm in the range 150 to 4000 cm^{-1}. HERMLE (Z-366) centrifuge machine (Germany) and Elmasonic (E 60 Hz) sonication bath was used for the washing and preparation of nanocomposite. Sensodirect Lovibond pH meter was used for buffer solution preparation. For the drying of samples, vacuum oven was used.

2.2.2. Electrochemical analysis

All the electrochemical analysis were carried on Gamry electrochemical workstation (Reference 3000/3000AE Potentiostat/Gaslvanostat/ZRA) made in USA. Cyclic voltammetry (CV), differential pulse voltammetry (DPV) and potentiostatic electrochemical impedance spectroscopy (EIS) were performed using Gamry instrument. Cyclic voltammetry was performed in the range of −0.3 to 0.8 V for both the determination of surface area studies and sensitivity of dopamine. The differential pulse voltammetry (DPV) was taken at step size of 2 mV, sample period of 1 s, pulse time of 0.5 s and pulse size of 50 mV. EIS measurements were taken w.r.t open circuit potential (OCP) at a frequency range of 100 kHz (initial frequency) to 0.1 Hz (final frequency), sweep rate of 50 mV/s, AC (alternating current) voltage of 10 mV rms and at a voltage of 0.287 V. Electrodes used during the study include modified/unmodified glassy carbon electrode (GCE) as a working electrode (W.E.) with a geometric surface area of 0.07 cm^2, Ag/AgCl (silver/ silver chloride with 0.3 M saturated potassium chloride solution) as a reference electrode (R.E.) and platinum wire as a counter electrode (C.E.). pH meter was used to monitor the pH of the buffer prepared solutions. Nitrogen gas was bubbled every time through the solutions for 5 min before conducting the electrochemical analysis.

2.3. Methodology

2.3.1. Synthesis of 5,10,15,20-Tetrakis(4-methoxyphenyl)porphyrin (TMePP) and copper 5,10,15,20-Tetrakis(4-methoxyphenyl)porphyrin (CuTMePP)

Tetramethoxyphenylporphyrin was synthesized by condensation of pyrrole and *para*-methoxybenzaldehyde following Adler Longo method (Adler et al., 1967) with some modification. Solution of freshly distilled pyrrole (8.6 mL; 0.12 mol) and 4-methoxybenzaldehyde (17.5 mL; 0.14 mol) in dimethylformamide was added slowly to the already refluxing propanoic acid (220.0 mL; 2.93 mol at 145 °C) the reaction mixture was refluxed for 1 h. Progress of the reaction was monitored by thin layer chromatography. Upon completion of the reaction the crude product in the flask was allowed to cool under dark. The product, TMePP, was isolated by filtration, subsequently washing with methanol and de-ionized water. The purple colored TMePP crystals were dried under vacuum at 45 °C for 24 h (yield = 28 %) (Phromsatit et al., 2016). The structure of TMePP is shown in Fig. S1 (a).

CuTMePP was synthesized by the metalation of tetramethoxyphenylporphyrin (TMePP). The solution of TMePP (794.0 mg in 50.0 mL DMF) and copper acetate (181.6 mg in 25.0 mL DMF) were placed together in a round bottom flask along with pyridine (1.0 mL) and refluxed at 150 °C for 4 hrs. Progress of the reaction was monitored by TLC as well as UV–visible spectroscopy which indicated reduction of number of Q-bands from four to two. Pure CuTMePP (yield 75 %) was obtained after performing column chromatography using chloroform and *n*-hexane (1:1) as solvent system with silica gel as stationary phase. Fig. S1 (b) represents the structure of CuTMePP.

2.3.2. Nanocomposite preparation

Carbon nanocoils (CNCs) were employed to prepare the nanocomposites for electrochemical analysis. For the preparation of CNCs/CuTMePP, a solution of CuTMePP (15.0 mg in 10.0 mL DMF) was added slowly to the CNCs dispersion (5.0 mg in 5.0 mL DMF) then the reaction mixture was sonicated for 1 h at room temperature and stirred for another 24 h to accomplish favorable interaction between CuTMePP and CNCs in the form of a composite. The product, CNC/CuTMePP, was obtained after removing DMF, washing with ethanol to get rid of any loosely attached residual CuTMePP using centrifuge machine. The nanocomposite was further dried under vacuum at 50 °C for 24 hrs. The CNC/TMePP nanocomposite was prepared in the same way for the comparison studies.

The CNC/CuTMePP ink was prepared by sonicating 2.0 mg of CNC/CuTMePP nanocomposite in 0.5 mL of DMF till a neat and stable dispersion was formed in about 40 min. Similarly, the inks of CNCs, TMePP, CuTMePP, and CNC/TMePP were also prepared in dimethylformamide. All the inks were stored in the refrigerator till further use.

2.3.3. Fabrication of the electrodes

Initially the glassy carbon electrode was polished with diamond and alumina slurry and then washed by sonication in

water and ethanol alternatively for three times for 2 min in each solvent. Finally, the electrode was washed with acetone once and dried in air. For the preparation of CNC/CuTMePP/GC, 8.0 μL of the CNC/CuTMePP nanocomposite ink was placed on the glassy carbon electrode and dried in air. In the same manner, CNCs/GCE, TMePP/GC, CuTMePP/GC and CNC/TMePP/GC electrodes were also fabricated.

3. Results and discussion

UV–visible spectroscopic analysis is one of the most essential and informative techniques in the porphyrin chemistry owing to its intense light absorbing nature. Fig. 1 represents the UV–visible spectra of the pristine materials as well as of the nanocomposites. The UV–vis. spectra of TMePP and CuTMePP have two distinct regions with intense Soret bands that appear at 420 nm and 418 nm, respectively owing to the π to π* electronic transitions between S_0 to S_2. The other is the Q absorption band region that corresponds to the electronic transitions taking place between HOMO to LUMO orbitals. In case of TMePP, four Q bands exist at 518 nm, 555 nm, 596 nm and 651 nm corresponding to S_0 to S_1 electronic transitions (Fig. 1: the green-colored band in inset). Upon metalation of TMePP with copper ions in CuTMePP, the number of Q bands are lessened to two at 540 nm and 580 nm that confirms the synthesis of CuTMePP (Fig. 1: the red-colored band in inset). As α band (Q band at 540 nm) is greater than β so it can be inferred that CuTMePP is a stable complex possessing a square planar geometry. The Q bands in CuTMePP exhibit bathochromic shift as compared to TMePP whereas the Soret band exhibit hypsochromic shift. Thus the insertion of metals in the cavity of tetraphenylporphyrins largely affect their UV–vis. spectra as compared to the free base tetraphenylporphyrin (Giovannetti, 2012).

Further, the UV–vis. spectra of CNC nanocomposites with TMePP and CuTMePP in 1:3 composition show the characteristic absorption bands of TMePP and CuTMePP except for shifting in the Soret band and few nanometers bathochromic shift is observed in the Q bands. In Fig. 1, it can be seen that a significant hypochromic effect exists in the Soret band of the CNC/TMePP and CNC/CuTMePP nanocomposites as compared to individual metallated and non-metallated methoxytetraphenylporphyrin. Thus, it can be inferred that an adequate pi-pi interaction was developed in the nanocomposites between the pi electrons of CNCs and the porphyrin core. The absorption peak for CNCs appearing at 263 nm is shown in Figure 1 and S2. The Soret band (418 nm) in CuTMePP is shifted to 417 nm in CNC/CuTMePP whereas the Q bands of CuTMePP undergo bathochromic shift towards 551 nm and 584 nm in the nanocomposite. Similarly, the Soret band of the CNC/TMePP appeared at 421 nm as compared to TMePP (420 nm) and the Q bands are shifted to 517 nm, 556 nm, 600 nm and 645 nm. UV–visible spectra depict the formation of nanocomposites of CNC with TMePP and with CuTMePP as the bathochromic shift exists in the Q bands of TMePP and CuTMePP when they are combined with carbon nanocoils thus a bathochromic shift in the spectra is evidence of pi-pi stacking of molecules with CNC.

Fig. 2 pictures the FTIR spectra for comparison of TMePP, CuTMePP, CNC, CNC/TMePP and CNC/CuTMePP. In the FTIR spectrum of TMePP, there is weak absorption characteristic band in TMePP i.e. 3312 cm^{-1} that corresponds to stretching vibration of N—H (Castro et al., 2015) and other stretching vibrations for aromatic = C—H, methoxy C—H, C=C, C=N, aryl—O—C (*asym*), alkyl C—O (*sym*), C—N and C=N appeared at 3027 cm^{-1}, 2960 cm^{-1}, 1590 cm^{-1}, 1350 cm^{-1}, 1259 cm^{-1}, 1019 cm^{-1}, 1190 cm^{-1}, respectively and N—H wagging vibration appears at 960 cm^{-1}. The bands for N—H stretching and wagging vibrations (Kowalczuk and Pitucha, 2019) in TMePP were disappeared when copper ion was incorporated into the CuTMePP macrocyclic ring. An extra band at 999 cm^{-1} in CuTMePP, ascribed to the stretching vibration of Cu-N bond that is a characteristic signal of CuTMePP (Neti et al., 2015). It is noted that all the other bands for stretching vibrations for aromatic = C—H, methoxy C—H, C=C, C=N, aryl—O—C (asymmetric), alkyl C—O

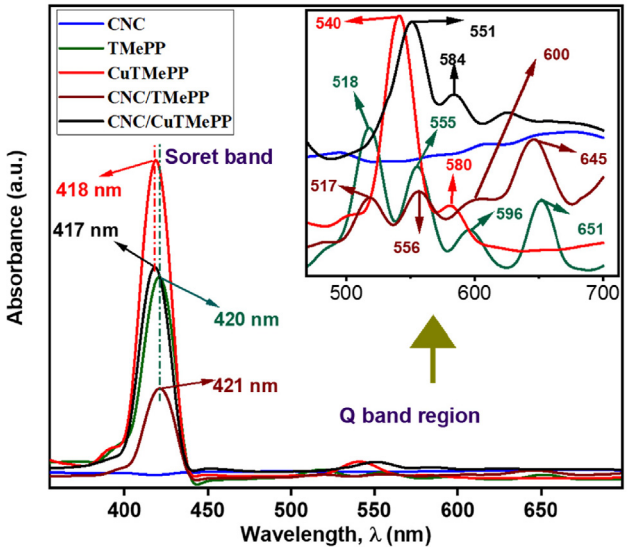

Fig. 1 UV–visible spectra of CNC, TMePP, CuTMePP, CNC/TMePP and CNC/CuTMePP. Inset: Q bands shown at higher magnification.

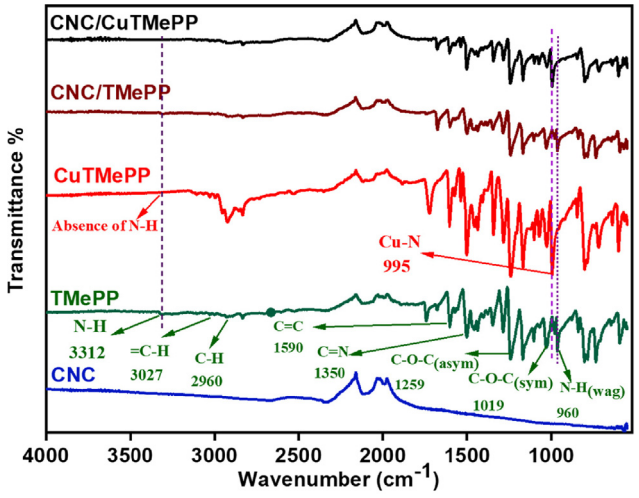

Fig. 2 FTIR spectra (b) of CNC, TMePP, CuTMePP, CNC/TMePP and CNC/CuTMePP.

(symmetric), C—N and C=N are present in CuTMePP but slightly shifted as compared to TMePP. The affirmation for the formation of TMePP and CuTMePP was done by these observations made on the basis of FTIR spectra. Further the FTIR analysis of CNC/TMePP and CNC/CuTMePP demonstrates a marked decrease and shifting of the bands that depicts a good non-covalent interaction has developed between carbon nanocoils and TMePP and carbon nanocoils and CuTMePP. As CNC do not contain any characteristic functional group except -C=C- structure so no other prominent bands are observed in their FTIR spectrum.

Raman analysis was performed for CNC and it showed the presence of D band and the G band (Ding et al., 2015; Deng et al., 2019) that are the characteristic bands of carbon nanostructures as shown in Figure S3. Two main peaks are present in the Raman spectrum of CNC at 1332 cm^{-1} and 1603 cm^{-1} which are designated as D band (speaks about the presence of amorphous carbon or sp^3 character) and G band (tells about presence of sp^2 hybridized carbon), respectively and the ratio of D to G band heights (I_D/I_G) tells about the more amorphous and polycrystalline nature of carbon nanocoils (Cui et al., 2014).

The XRD spectra of CNC, CuTMePP and CNC/CuTMePP are shown in Figure S4. XRD of CNC/CuTMePP further confirms the formation of the nanocomposite as the shifting of diffraction peaks is observed in the nanocomposite as compared to the pristine CNC and CuTMePP. The prominent amorphous peak at $2\theta = 21.5°$ (0 0 2) is the characteristic peak for the diffraction of carbon (JCPDS No. 26–1077) that is present in all the three samples but with slight shifting in the CNC/CuTMePP nanocomposite. The presence of 020 (prominent peak) and 121 planes at $2\theta = 6.06°$ and 12.41°, respectively with some other small peaks in CuTMePP tells about the partially crystalline solid (El-Nahass et al., 2014) and further these peaks are shifted in the composite confirms the formation of CNC/CuTMePP nanoarchitecture.

Transmission electron miscrosopy (TEM) image of pure CNC in Fig. 3 (a) shows the compact coiled and hollow tubular internal structure of CNC. SEM image for pure CNC is also shown in Fig. 3 (b) revealing the presence of only coiled structures and the pristine CuTMePP (Fig. 3 (c)) depicts the presence some aggregated sheet like structures.

SEM images of the CNC/CuTMePP nanocomposite are shown in Fig. 3 (d) and its inset at high and low resolutions of 5 μm and 0.5 μm, respectively. It can be seen that carbon nanocoils are attached to molecular aggregated sheets of CuTMePP. EDS of CNC (Figure S5) shows presence of carbon (85.5 wt%) and oxygen (14.5 wt%) and the EDS of CuTMePP exhibits carbon (66.4 wt%), oxygen (15.1 wt%), nitrogen (11.8 wt%) and copper (6.8 wt%). The EDS spectrum of CNC/CuTMePP in S5 illustrates presence of carbon, oxygen, nitrogen and copper in weight percent of 72.3 %, 10.0 %, 9.8 % and 7.9 %, respectively. The presence of Cu in the nanocomposite indicates the development of supramolecular assortment of CuTMePP and CNC.

Electrochemical activities of the electrodes.

The electrochemical properties of the GC, CNC/GC, TMePP/GC, CuTMePP/GC, CNC/TMePP/GC, CNC/CuTMePP/GC electrodes were determined by performing cyclic voltammetry (CV) and electrochemical impedance spectroscopic (EIS) analysis in 5 mM potassium ferricyanide ($K_3[Fe(CN)_6]$) standard solution, which was prepared in 0.1 M potassium phosphate buffer and 0.1 M potassium chloride solution an auxiliary electrolyte. Cyclic voltammograms in Fig. 4 (a) demonstrate an excellent electrochemistry of CNC/CuTMePP/GC electrode in terms of efficient electrochemical activity of the CuTMePP supported on carbon nanocoils from ferro-/ferricyanide couple by mediating a fast and enhanced electron transfer to the glassy carbon electrode that is detected in the form of reversible redox current. CNC/TMePP/GC and CNC/GC also exhibited reversibility and good redox peak current but less than CNC/CuTMePP and greater than GC, CuTMePP/GC and TMePP/GC. The low onset potential accompanied with a higher peak current also tells about the catalytic behavior of the electrodes. CNC/CuTMePP/GC exhibits an onset potential of 0.07 V that is more negative than the onset potential possessed by the CNC/TMePP/GC, CNC/GC, CuTMEPP/GC, TMePP/GC and GC as 0.11 V, 0.14 V, 0.17 V, 0.19 V and 0.213 V, respectively. Thus, CNC/CuTMePP/GC is synergistically playing a role in the efficient charge transfer activity in the form of composite. Further the electroactive surface area (ESA) of all the electrodes was determined by employing Randles-Sevcik equation (A):

$$I_{pa} = 2.69x10^5 n^{3/2} A D^{1/2} C \upsilon^{1/2} \text{(A)}$$

where, I_{pa} is the current in amperes, n is the number of electrons, A is the effective electrode area in cm^2, D is the diffusion coefficient of potassium ferricyanide in cm^2s^{-1}, C is the concentration in $molcm^{-3}$ and υ is the scan rate in Vs^{-1} and the unit for the constant is $Cmol^{-1}V^{-1/2}$) and CNC/CuTMePP/GC showed highest ESA of 0.068 cm^2 as compared to other prepared electrodes as shown in Table S1. The electrode interfacial properties obtained from the EIS, are presented in Fig. 4 (b). The EIS extracted data in the form of Nyquist plot provides an information about charge transfer resistance (R_{ct}) and diffusion limited process. The R_{ct} values determined from the Nyquist data after performing simplified Randles circuit analysis for the fabricated electrodes, GC, CNC/GC, TMePP/GC, CuTMePP/GC, CNC/TMePP/GC, and CNC/CuTMePP/GC, were 11.89 kΩ, 761.1 Ω, 8.13 kΩ, 14.12 kΩ, 2.256 kΩ and 456.1 Ω, respectively. The Randles circuit consist of charge transfer resistance (R_{ct}), solution ohmic resistance (R_s) and double layer capacitance (C_{dl}). To compare the performance of the modified electrodes, the same circuit was applied to analyze the EIS curves. Among all the prepared electrodes, CNC/CuTMePP/GC exhibited the least electron transfer resistance thus more conductive in nature. The enhanced electrochemical properties of CNC/CuTMePP/GC are due to the synergistic catalytic properties and large surface area possessed by CuTMePP/CNC/GC.

The values of charge transfer resistance, R_{ct} (kΩ) obtained from EIS, electroactive surface area A (cm^2) obtained from the above CV studies can be utilized to determine the standard heterogeneous rate constant k^0 (cm/s) of all the electrodes by the following equation (Nia et al., 2019; Setoudeh et al., 2020):

$$k^0 = \frac{RT}{R_{ct}F^2CA} \text{(B)}.$$

Where, F is the Faradays constant (C/mol), R is the ideal gas constant (J/Kmol) and T is the temperature (K). Hence, the values of heterogeneous rate constant calculated for GC, CNC/GC, TMePP/GC, CuTMePP/GC, CNC/TMePP/GC and CNC/CuTMePP/GC are 0.29×10^{-3}, 1.35×10^{-3}, 0.47×10^{-3}, 0.42×10^{-3}, 0.36×10^{-3} and 1.72×10^{-3} cm/s,

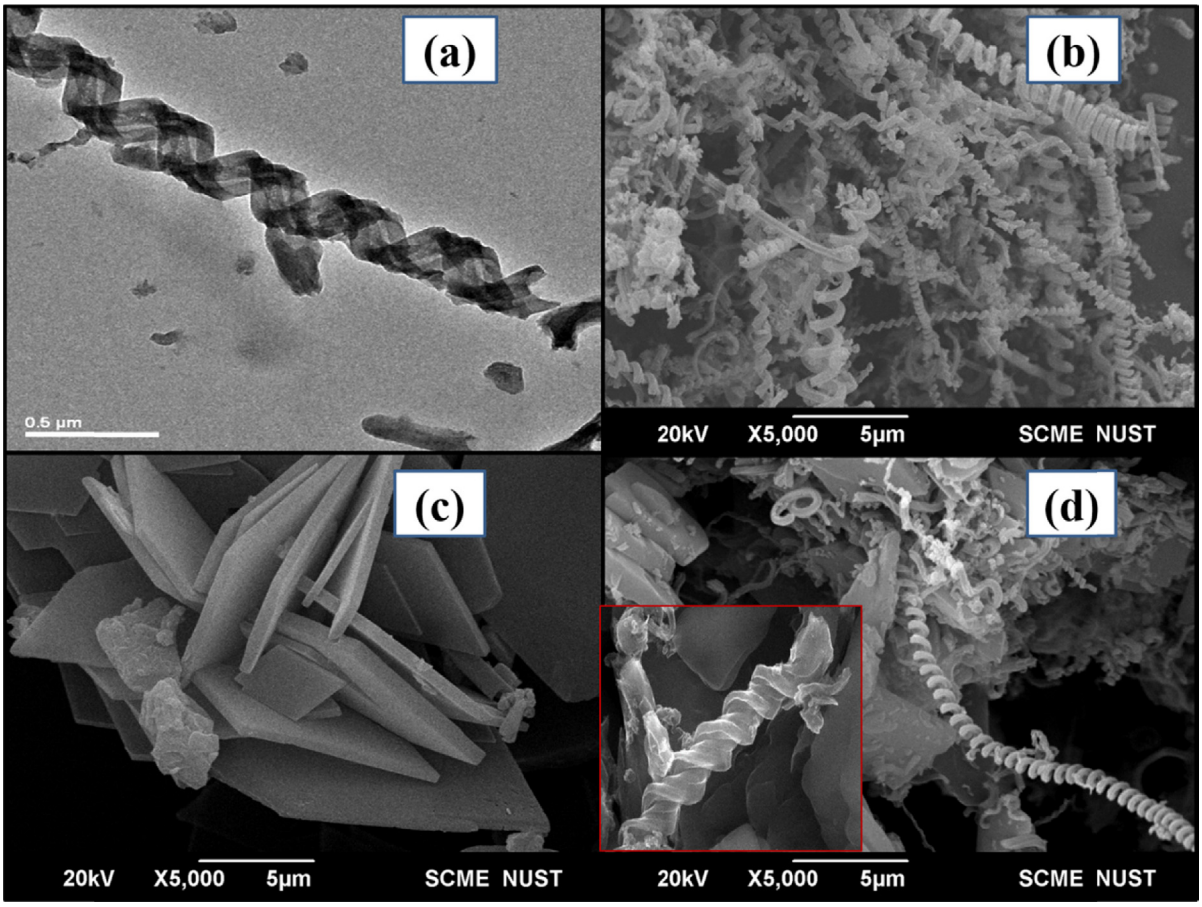

Fig. 3 TEM image of CNC at 0.5 µm (a) and SEM images of CNC (b), CuTMePP (c) and CNC/CuTMePP nanocomposite (d) at 5 µm. Inset of (d) shows SEM image CNC/CuTMePP nanocomposite at 0.5 µm.

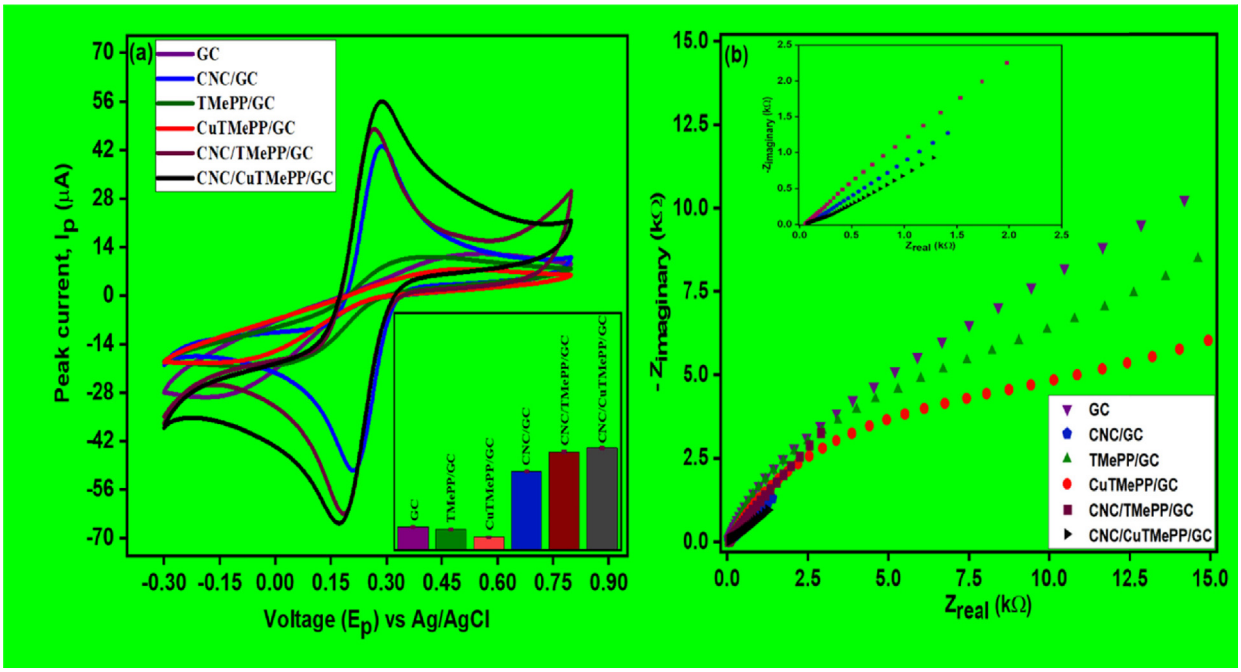

Fig. 4 Cyclic voltammetry analysis (a) and Nyquist plots (b) of GC, CNC/GC, TMePP/GC, CuTMePP/GC, CNC/TMePP/GC and CNC/CuTMePP/GC performed in 5 mM potassium ferricyanide. Inset (a): Bar graph for the all the electrodes (n = 3).

respectively. The value of rate constant provides an information of the kinetics of the electrode in terms of its electrocatalytic feasibility to electrochemically detect analyte via redox process. Higher the value of k^0, lesser the time is required for the establishment of equilibrium as compared to the lower values of heterogeneous rate constant. Low k^0 value indicates the slow electron transfer. Hence, it is concluded that CNC/CuTMePP/GC exhibits higher k^0 as compared to other modified GC electrodes so it possesses favorable properties that can be used for the electrochemical detection of analyte.

3.1. Exploration of the Best Sensor

Cyclic voltammetry was utilized to determine the electrochemical sensing ability of the bare glassy carbon electrode (GC), TMePP/GC, CuTMePP/GC, CNC/GC, CNC/TMePP/GC and CNC/CuTMePP/GC modified electrodes in 0.5 mM dopamine (0.1 M potassium phosphate buffer, pH 7). The potential window selected was in the range from −0.3 to 0.8 V with scan rate of 0.05 V/s. The comparison of the voltammograms present a clear picture about the interaction of DA with electrode surface (Fig. 5). For DA very weak oxidation peak current was observed at higher potential values with broad peaks for GC (I_{pa} = 5.73 μA; E_{pa} = 433 mV), TMePP/GC (I_{pa} = 2.34 μA; E_{pa} = 370 mV) and CuTMePP/GC (I_{pa} = 5.93 μA; E_{pa} = 525 mV) which was due to the sluggish redox process, less charge transfer ability and poor transduction mechanism of these electrodes. Thus, the process of detection of DA at these electrodes is reversible. While CNC/GC (I_{pa} = 7.74 μA; E_{pa} = 205 mV) showed well defined redox peak indicating good interaction with dopamine. When the CV was performed with CNC/TMePP/GC and CNC/CuTMePP/GC the redox peaks appeared at narrower and decreased peak potential with enhanced peak currents. CNC/TMePP/GC showed an anodic peak current of 13.18 μA for DA at E_{pa} of 203 mV. CNC/CuTMePP/GC with an I_{pa} of 15.1 μA at E_{pa} of 192 mV, catalyzes dopamine by extracting the two electrons cum two protons from the hydroxyl groups and oxidizes it to dopamine-o-quinone. The peak potential difference (E_{pa} –E_{pc} = ΔE_p) between the anodic peak and the cathodic peak of the electrodes illustrates the electrocatalytic capability. ΔE_p calculated for CNC/CuTMePP/GC, CNC/TMePP/GC and CNC/GC are 49 mV, 56 mV and 60 mV, respectively. Increased Ipa and low ΔEp for CNC/CuTMePP/GC shows a significant electrocatalytic ability of the electrode towards dopamine due to its high surface area, greater electron charge transfer ability and presence of catalytic centres. The proposed mechanism for the dopamine redox process is shown in Fig. S6.

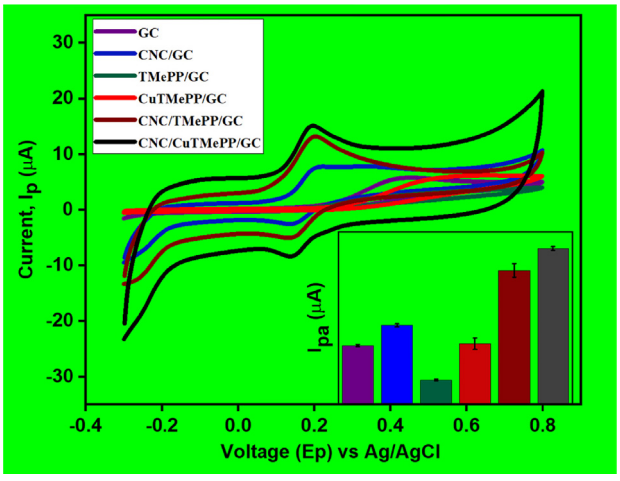

Fig. 5 Cyclic voltammetry analysis of GC, CNC/GC, TMePP/GC, CuTMePP/GC, CNC/TMePP/GC and CNC/CuTMePP/GC performed in 0.50 mM dopamine (0.1 M potassium phosphate buffer, pH 7.0, scan rate = 0.05 V/s).

CNC/CuTMeP/GC has demonstrated to be the superior electrocatalyst for dopamine therefore, it is subjected for further optimization studies. Optimum pH for the sensor, CNC/CuTMePP/GC, was determined by analyzing DA at pH 5.0, 6.0, 7.0 and 8.0 in 0.1 M aqueous potassium phosphate buffer. The electro-redox process of dopamine is highly responsive to pH due to the presence of catechol moiety. The CV and DPV revealed (Fig. 6 (a) and (b)) that dopamine oxidation produces maximum current at pH 7.0 as compared to pH 5.0, 6.0, or 8.0. Subsequently pH 7.0 was used for further studies. The negative transposition of peak potential was observed in concurrent to the change of pH from 5.0 to 8.0 and when a plot between anodic peak potential (E_{pa}) and pH of the solution was made (shown in insets of Fig. 8 a and b as blue lines) the slope came out to be 0.080 V/pH (CV) and 0.077 V/pH (obtained using DPV) with R^2 values of 0.99 and 0.99, respectively. The slopes obtained from CV and DPV are close to the theoretical value 0.059 V/pH (theoretical Nernst value) and tell us about the involvement of equal number of protons and electrons in the electro-redox process of dopamine occurring at the surface of the CNC/CuTMePP/GC electrode.

The change in the redox peaks as a function of the scan rate was studied to observe the kinetic behavior of DA detection at the electrode interface. Different sweep rates were applied ranging from 0.005 V/s to 0.2 V/s. Fig. 7 (a) and (b) shows that I_{pa} and I_{pc} are considerably raised with an increasing scan rate. A calibration plot was constructed between redox peak currents (I_{pa} or I_{pc}) and square root of the scan rate, $\upsilon^{1/2}$ $(mV/s)^{1/2}$ by applying the straight-line equation the value of R^2 appeared to be 0.99 (I_{pa}) and 0.97 (I_{pc}) thus representing a diffusion controlled process. The regression equations are shown below as (B) and (C):

$$I_{pa}(\mu A) = 5.95\left(\upsilon^{1/2}\right) - 17.05\left(R^2 = 0.99\right)(B).$$

$$I_{pc}(\mu A) = -4.22\left(\upsilon^{1/2}\right) + 14.36\left(R^2 = 0.97\right)(C).$$

The plot of I_{pa} (or I_{pc}) versus scan rate (υ) revealed the regression coefficient to be 0.99 (I_{pa} (μA) = 0.27 (υ) + 13.47) and 0.98 (I_{pc} (μA) = -0.24 (υ) −1.92), indicating the transport of dopamine is also adsorption controlled phenomenon (shown in Figure S7 a). Thus, it is further concluded that the interfacial interaction of DA with CNC/CuTMePP/GC is both diffusion controlled cum surface adsorption process. Moreover, the value of slope of ln I_{pa} versus natural log of scan rate (ln υ) is 0.63 (shown in Figure S7 b) which is greater than 0.5 (the ideal value for diffusion-limited process) and less than 1 (the ideal value for surface controlled process), provides an evidence that the major process is diffusion controlled with a little contribution of adsorption-controlled process (Gnahore et al., 2017).

The number of electrons (n) involved in the redox process of dopamine has been calculated using the Laviron method (Peik-See et al., 2014; Guo et al., 2019). The two linear calibra-

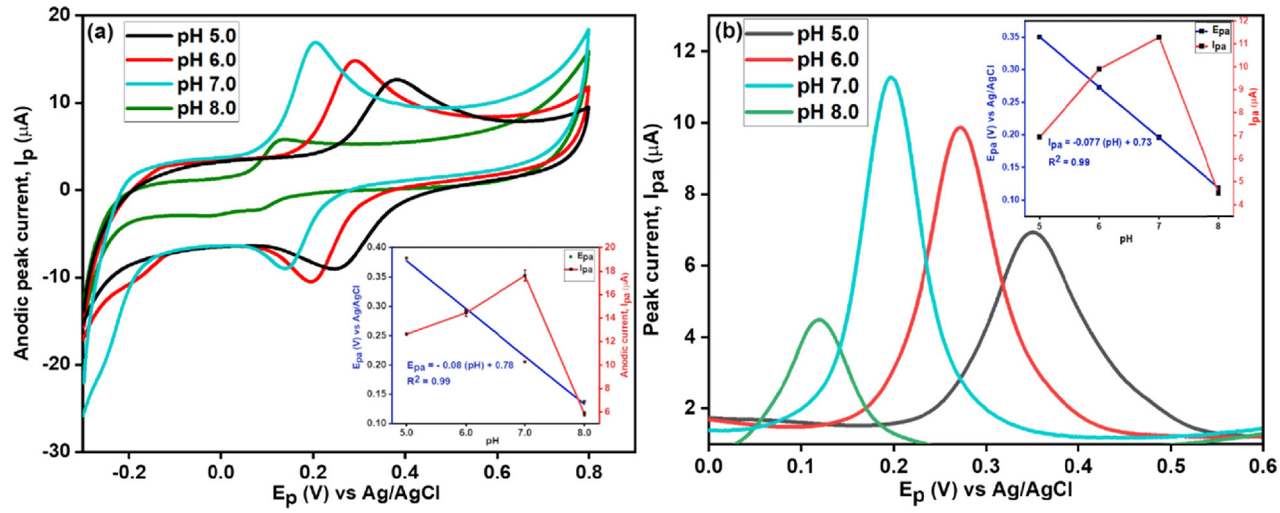

Fig. 6 CV (a) and DPV (b) of CNC/CuTMePP/GC towards 0.5 mM dopamine at pH 5.0, 6.0, 7.0 and 8.0; Insets: Relation between E_{pa} and pH (blue lines) and between I_{pa} and pH (red lines).

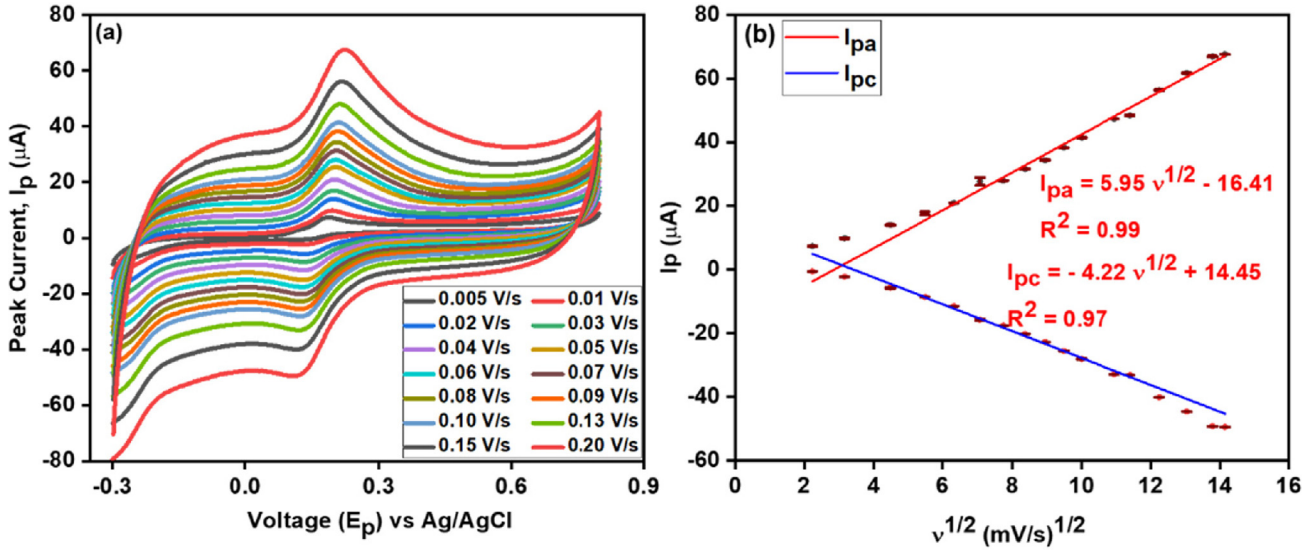

Fig. 7 Effect of different scan rates (a) at CNC/CuTMePP/GC performed in 0.5 mM dopamine (potassium phosphate buffer 0.1 M, pH 7.0); and calibration plot (b) between redox current and square root of scan rate.

tion plots of anodic and cathodic peak potential versus log of scan rate has been developed (Figure S7 c) and the values of cathodic or anodic slopes are used to determine the value of transfer co-efficients $\alpha_{c \text{ and }} \alpha_a$ which are further used to determine the value of n. The number of electrons involved in the redox process of dopamine are $2.2 \approx 2$.

3.2. Concentration study

The behavior of newly designed CNC/CuTMePP/GC electrode was studied by varying the concentration of dopamine i.e. 0.1 μM to 800.0 μM (Fig. 8). A rise in the peak current was observed with the increase of concentration of dopamine in 0.1 M phosphate buffer of pH 7.0 at a fixed scan rate of 0.050 V/s.

The effect of change of concentration was studied in the range of 0.1 μM to 800.0 μM and LoD was obtained in two linear ranges extending from 0.1 μM to 100.0 μM and 100.0 μM to 800.0 μM with regression equations I_{pa} (μA) = 0.12 (μM) + 1.03 (R^2 = 0.99) (Fig. 8: inset and I_{pa} (μA) = 0.014 (μM) + 10.03 (R^2 = 0.96) (Fig. 8: inset b), respectively. The limit of detection (LoD), by using the formula 3 × (standard deviation of the blank / slope of the concentration), was found to be 50.0 nM in a linear range of 0.1 μM to 100.0 μM. Similarly, the limit of quantification (LoQ) was determined to be 167.0 nM by using the equation i.e. 10 × (standard deviation of the blank / slope of the concentration). Sensitivity of the electrode is another very important factor to be considered in the electrochemical sensing studies, which can be obtained by relating the slope obtained from the concentration studies to that of the surface area of the electrode as: slope/0.068 cm^2. The sensitivity of CNC/CuTMePP/GC for dopamine is 1.76 $\mu A \mu M^{-1} cm^{-2}$ in the linear range of 0.1 μM to 100.0 μM. LoD, LoQ and sensitivity obtained in

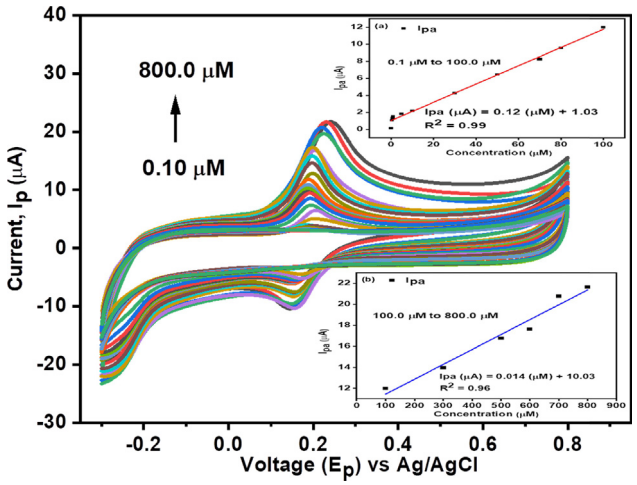

Fig. 8 Cyclic voltammetry of CNC/CuTMePP/GC towards 0.1 to 800.0 µM dopamine in 0.1 M, pH 7.0 potassium phosphate buffer at a scan rate of 0.05 V/s. Inset: Effect on anodic peak current as a function of change in concentration of dopamine in linear ranges of 0.1 to 100.0 µM (a) and 100.0 to 800.0 µM (b).

the concentration range varying from 100.0 µM to 800.0 µM were 428.0 nM, 1.42 µM and 0.21 $\mu A \mu M^{-1} cm^{-2}$, respectively.

Differential pulse voltammetric analysis was performed to examine the behavior of CNC/CuTMePP/GC electrode towards varying concentrations of dopamine in 0.1 M potassium phosphate buffer because it is the more sensitive electroanalytical technique as compared to cyclic voltammetry to study the electrode surface bound analytes (Ensafi et al., 2009). The concentration range studied ranges between 0.1 and 800.0 µM dopamine as shown in Fig. 9. The anodic peak current heightens as the concentration of dopamine increases in the buffer. Two linear ranges were obtained. Limit of detection obtained through DPV in a linear range of 0.1 to 100.0 µM (Fig. 9: inset a) is 64.0 nM with a sensitivity of 0.75 $\mu A \mu M^{-1} cm^{-2}$. LoQ was also determined as 211.0 nM. In the linear range of 100.0 to 800.0 µM (Fig. 9: inset b) the LoD, LoQ and sensitivity of the electrode were found to be 249.0 nM, 830.0 nM and 0.19 $\mu A \mu M^{-1} cm^{-2}$, respectively.

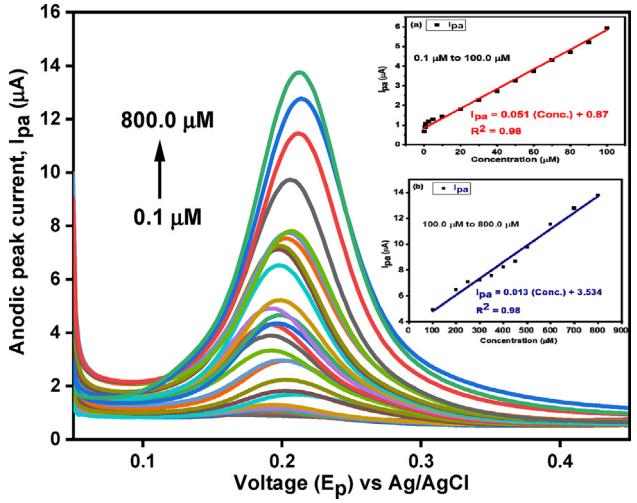

Fig. 9 DPV analysis of CNC/CuTMePP/GC towards 0.1 to 800.0 µM DA concentration. Inset: Effect on anodic peak current as a function of change in concentration of dopamine in linear ranges of 0.1 to 100.0 µM (a) and 100.0 to 800.0 µM (b).

3.3. Reproducibility

Three different electrodes were prepared (CCTG-1, CCTG-2 and CCTG-3) under identical conditions by loading 8.0 µL ink of CNC/CuTMePP on the glassy carbon electrodes. The electrochemical sensing of the electrodes was performed in 0.5 mM DA. Results obtained matched well and a deviation in the sensitivity between these electrodes was 4.93 %. It suggests an efficacy in the sensing of dopamine using CNC/CuTMePP/GC either in different environmental or handling conditions. CNC/CuTMePP proved to be an active nanocomposite to detect DA. The slight variation in sensitivity could be due to the difference in the conductivity of the glassy carbon electrodes, film thickness of the nanocomposite deposited on GCs and evaporation rate of the solvent from the surface of the electrode. The activity of CCTG-1, CCTG-2 and CCTG-3 is shown in the form of bar graph in Fig. 10.

3.4. Stability studies

Stability studies were performed by using two methods; in the 1st method the intraday stability test (repeatability studies) i.e. the electrode was prepared and ten CV and ten DPV experiments were conducted in 0.50 mM DA (0.1 M potassium phosphate buffer pH 7) and 3.01 % and 2.36 %, relative standard deviation (RSD) was calculated, respectively (Fig. 11). These values suggest significant stability performance of the electrode.

In the second method the same electrode CNC/CuTMePP/GC was stored in potassium phosphate buffer (pH 7) in the refrigerator (4 °C) to monitor the inter-day stability and the stability test was performed for over a period of two weeks. A current loss of 15.48 % was observed at the twelfth day as compared to the first day (Fig. 12). An increase in the current

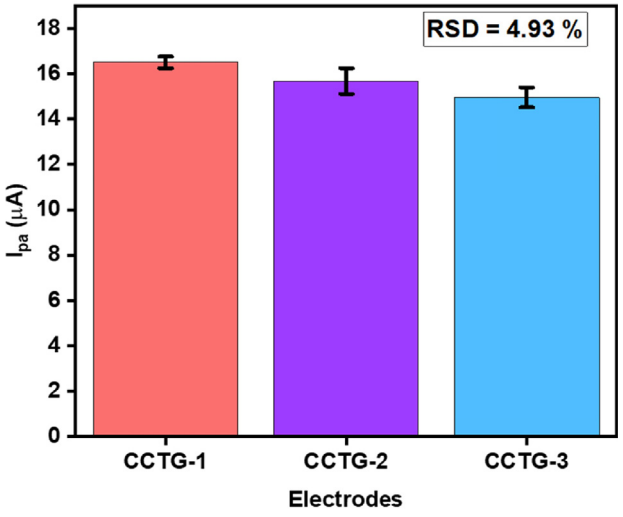

Fig. 10 Results of reproducibility studies at three different electrodes in 0.50 mM DA (0.1 M PBS buffer, pH 7).

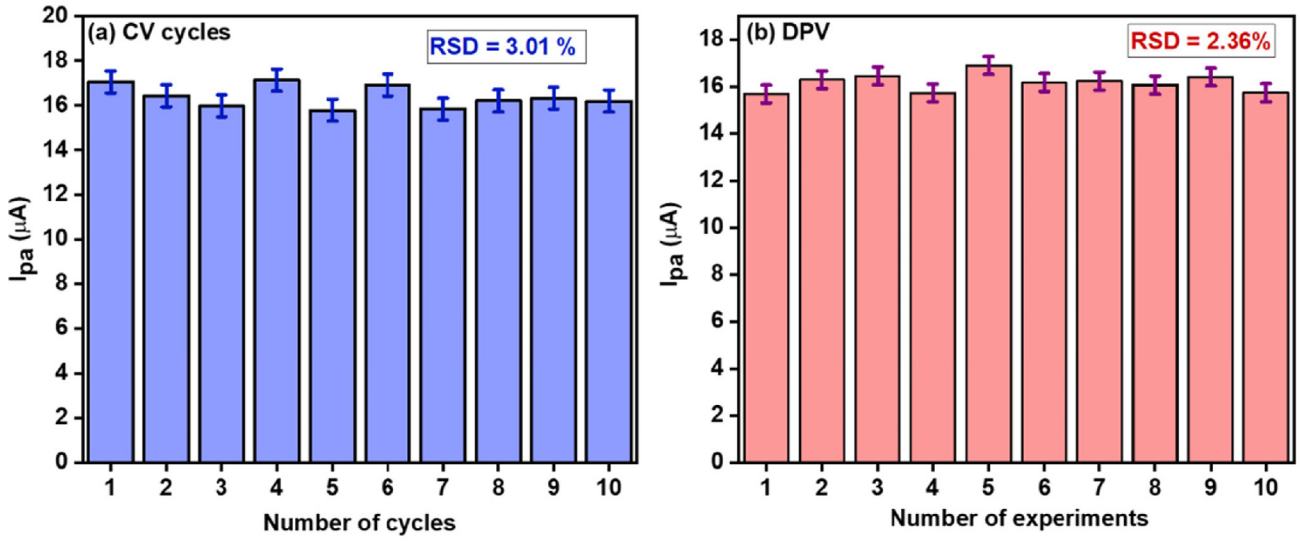

Fig. 11 Intraday stability studies of CNC/CuTMePP/GC using CV (a) and DPV (b) in 0.50 mM DA (0.1 M potassium phosphate buffer, pH7).

on the fourth day could be due to some adsorption controlled process of the DA on the surface of CNC/CuTMePP/GC.

3.5. Interference studies

To monitor the interference effect of various biomolecules onto the sensing ability of CNC/CuTMePP/GC towards dopamine, 3-fold higher concentrations of amino acids, glucose, uric acid and ascorbic were added to 0.50 mM solution of dopamine (pH 7 buffer). Amino acids include leucine, glycine, proline, phenylalanine, and tyrosine. No notable interference regarding the increase or decrease in peak current was observed for the DA (Fig. 13). Similarly, when the ternary mixture of dopamine, ascorbic acid and uric acid was analyzed, no prominent change in the peak current of dopamine was observed. Thus, it is concluded that the sensor can selectively detect DA in biological samples at a fixed potential. Similarly, the effect of inorganic salts was also observed using KNO_3, $MgSO_4$, $CaCl_2$, Na_2CO_3 and $NaHCO_3$. No prominent interference was observed for the detection of dopamine in the presence of inorganic salts.

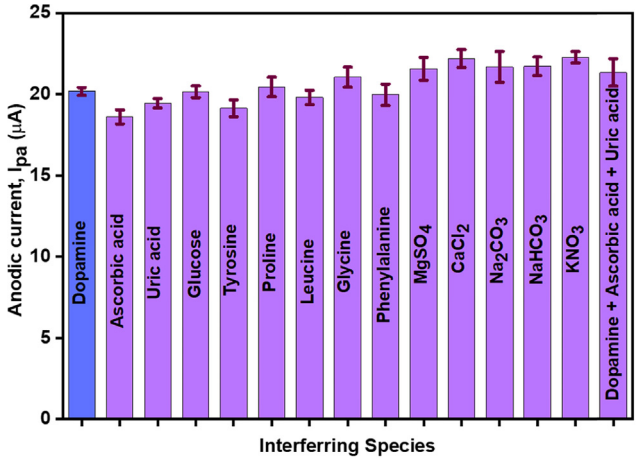

Fig. 13 Effect of different organic and inorganic compounds on the sensing study of dopamine using CNC/CuTMePP/GC (0.50 mM DA in 0.1 M phosphate buffer).

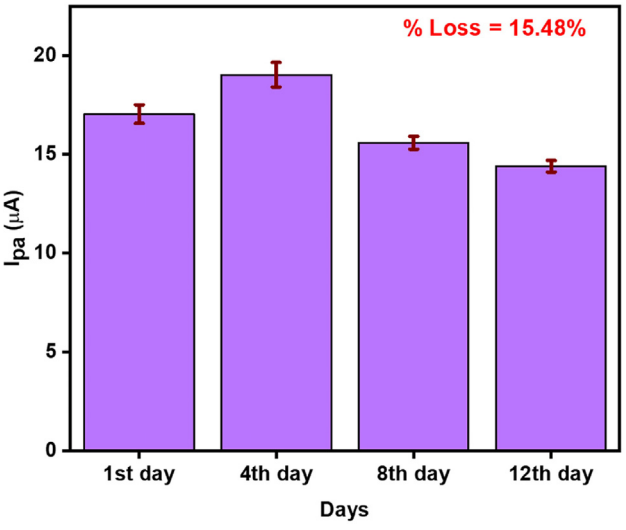

Fig. 12 Inter-day stability studies of CNC/CuTMePP/GC in 0.50 mM DA (0.1 M phosphate buffer, pH = 7) using DPV.

3.6. Comparison with the literature

Table 1 shows some of the previously reported DA sensors based on carbon nanostructures and their comparison with the present sensor in terms of LoD, sensitivity and linear range. Our sensor presented better performance and almost comparable performance with respect to LoD, sensitivity and concentration range with the sensor in which

Table 1 Comparison of previous reported carbon nanostructure-based electrodes with the CNC/CuTMePP/GC electrode for dopamine detection.

Sr.#	Electrode	LoD	Sensitivity	Linear range	Method	Ref.
1	[a]RGO/Mn-TPP/GCE	8.0 nM	2.606 μAμM^{-1}cm^{-2}	0.30 to 188.8 μM	Amperometry	(Sakthinathan et al., 2016)
2	[b]Porphyrin-rGO/ GCE	0.0095 μM	–	1.0 to 70.0 μM	DPV	(Lv et al., 2014)
3	[c]CuTPP/CRGO/GCE	0.76 μM	2.46 μAμM^{-1}cm^{-2}	2.0 to 200.0 μM	CV, DPV	(Karuppiah et al., 2016)
4	[d]RGO/Cu-TECP/GCE	0.58 μM	–	2.0 – 200.0 μM	DPV	(Huang et al., 2018)
5	[e]GQDs-MWCNTs /GCE	0.87 nM	–	0.005 to 100.0 μM	DPV	(Huang et al., 2020)
6	[f]f-MWCNT/AgNP	0.27 μM	–	0.0–0.8 μM	DPV	(Anshori et al., 2021)
7	CNC/Cu-TMePP/GC	50.0 nM	1.76 μA μM^{-1}cm^{-2}	0.1–100.0 μM	CV	Present work
		428.0 nM	0.21 μA μM^{-1}cm^{-2}	100.0–800.0 μM		
8	CNC/Cu-TMePP/GC	64.0 nM	0.75 μAμM^{-1} cm^{-2}	0.1 – 100.0 μM	DPV	Present work
		249.0 nM	0.19 μA μM^{-1} cm^{-2}	100.0 – 800.0 μM		

[a] RGO/Mn-TPP/GCE: Reduced graphene oxide/Manganese-tetraphenylporphyrin/Glassy carbon electrode.
[b] Porphyrin-rGO/ GCE: Protoporphyrin IX-rGO/GCE.
[c] CuTPP/RGO/GCE: Copper tetraphenylporphyrin/chemically reduced graphene oxide/GCE.
[d] RGO/Cu-TECP/GCE: Reduced graphene oxide/Tetrakis-(ethoxycarbonyl) porphyrin copper(II) supported glassy carbon electrode.
[e] GQDs-MWCNTs /GCE: Graphene quantum dots-multiwalled carbon nanotubes/GCE.
[f] f-MWCNT/AgNP: Functionalized MWCNT/silver nanoparticles deposited on carbon electrode.

tetraphenylporphyrin-carbon nanostructures were used i.e. Sr # 3 and Sr # 4.

3.7. Determination of Dopamine in Clinical Sample

The practical application of the sensor was performed in the human blood serum. The serum was diluted using 0.1 M potassium phosphate buffer solution by adding 230.0 μL of serum in 10.0 mL of the 0.1 M phosphate buffer. DA was added to the diluted serum in such a way to maintain the concentration of DA in the serum as 5.0 μM, 10.0 μM and 20.0 μM. CV and DPV were performed in the prepared serum samples. The results in Table 2 show the good % recovery of the DA in the serum and it is concluded that no contributing interference was observed by other species present in the serum. In the blank solution, no peak was observed in the potential range of −0.3 to 0.8 V, whereas a prominent redox peak for DA was observed at the same potential as for the standard DA solution. CNC/CuTMePP/GC fabricated electrode can be used for device fabrication for dopamine detection.

Table 2 Detection of dopamine in human blood serum using CNC/CuTMePP/GC.

Method	Concentration of DA added (μM)	Found (μM)	RSD %	% Recovery
CV	5.0	5.7	1.7	114.0
	10.0	10.3	1.04	103.7
	20.0	18.9	2.3	94.5
DPV	5.0	4.7	2.65	94.0
	10.0	9.9	2.5	99.0
	20.0	21.0	2.14	105.0

4. Conclusions

A dopamine sensor was developed from the functionalization of glassy carbon electrode surface by an assembly of carbon nanocoils attached copper tetramethoxyphenylporphyrin. The electrostatic interaction between CNC and TMePP was developed using a simple sonication protocol. For comparison studies, other electrodes such as CNC/GC, TMePP/GC, CuTMePP/GC and CNC/TMePP were also prepared using the same method i.e. drop-coating. CNC/CuTMePP/GC exhibited excellent electrochemical behavior towards dopamine detection in wide concentration range of 0.1 to 800.0 μM. CNC/CuTMePP/GC exhibits an effective surface area of 0.068 cm^2. To calculate the limit of detection (LoD), limit of quantification (LoQ) and sensitivity of the electrode two linear trends in concentrations were employed i.e. lower concentration ranges of 0 0.1 to 100.0 μM and higher concentration from 100.0 to 800.0 μM using both cyclic voltammetry and differential pulse voltammetry. In the lower concentrations, LoD, LoQ and sensitivity was obtained as 50.0 nM, 167.0 nM and 1.76 μAμM^{-1}cm^{-2}, respectively via cyclic voltammetry. Differential pulse voltammetry presented LoD, LoQ and sensitivity as 64.0 nM, 211.0 nM and 0.75 μAμM^{-1}cm^{-2}, respectively in a linear concentration range of 0.10 to 100.0 μM. CNC/CuTMePP/GC illustrated good intra/inter-day stabilities. Three different electrodes prepared by using our nanocomposite showed reproducible results in 0.50 mM DA. The electrode has also demonstrated excellent % recovery in the spiked human serum samples. According to the above information, the developed nanosensor could provide possibility to produce the clinical medical diagnosis device for determination of dopamine.

Funding Source

This research was supported by Pakistan Science Foundation (PSF-NSFC/Eng-C- NUST (03)).

CRediT authorship contribution statement

Syeda Aqsa Batool Bukhari: Methodology, Formal analysis, Writing – original draft, Investigation. **Habib Nasir:** Supervi-

sion, Conceptualization, Resources, Funding acquisition. **Effat Sitara:** Formal analysis. **Tehmina Akhtar:** Methodology. **Muhammed Ramazan Oduncu:** Formal analysis. **Sadia Iram:** Formal analysis. **Lujun Pan:** Supervision, Resources.

Declaration of Competing Interest

The authors declare that they have no known competing financial interests or personal relationships that could have appeared to influence the work reported in this paper.

Acknowledgement

Authors are thankful to National University of Sciences and Technology, Islamabad, Pakistan for providing lab facilities to carry out this project. We also acknowledge Pakistan Science Foundation for funding this research.

Appendix A. Supplementary data

Supplementary data to this article can be found online at https://doi.org/10.1016/j.arabjc.2022.104375.

References

Adler, A.D., Longo, F.R., Finarelli, J.D., et al, 1967. A simplified synthesis for meso-tetraphenylporphine. J. Org. Chem. 32, 476.

Anshori, I., Nuraviana Rizalputri, L., Rona Althof, R., et al, 2021. Functionalized multi-walled carbon nanotube/silver nanoparticle (f-MWCNT/AgNP) nanocomposites as non-enzymatic electrochemical biosensors for dopamine detection. Nanocomposites. 7, 97–108.

Anuar, N.S., Basirun, W.J., Shalauddin, M., et al, 2020. A dopamine electrochemical sensor based on a platinum–silver graphene nanocomposite modified electrode. RSC Adv. 10, 17336–17344.

Auwärter, W., Écija, D., Klappenberger, F., et al, 2015. Porphyrins at interfaces. Nat. Chem. 7, 105–120.

Baytak, A.K., Aslanoglu, M., 2020. A novel sensitive method for the simultaneous determination of ascorbic acid, dopamine, uric acid and tryptophan using a voltammetric platform based on carbon black nanoballs. Arabian J. Chem. 13, 1702–1711.

Bhakta, A.K., Mascarenhas, R.J., D'Souza, O.J., et al, 2015. Iron nanoparticles decorated multi-wall carbon nanotubes modified carbon paste electrode as an electrochemical sensor for the simultaneous determination of uric acid in the presence of ascorbic acid, dopamine and l-tyrosine. Mater. Sci. Eng., C 57, 328–337.

Castro, K.A., Silva, S., Pereira, P.M., et al, 2015. Galactodendritic porphyrinic conjugates as new biomimetic catalysts for oxidation reactions 54, 4382–4393.

Chen, F., Fang, B., Wang, S., 2021. A fast and validated HPLC method for simultaneous determination of dopamine, dobutamine, phentolamine, furosemide, and aminophylline in infusion samples and injection formulations. J. Anal. Meth Chem., 2021

Cui, R., Pan, L., Li, D., et al, 2014. Controlled synthesis of carbon nanocoils and carbon nanotubes on common paper substrates. Carbon 76, 455–458.

Davis, W., Slawson, R., Rigby, G., 1953. An unusual form of carbon. Nature 171, 756.

Deng, C., Wang, P., Li, C., et al, 2019. Effect of ethanol soaking on the structure and physical properties of carbon nanocoils. Diam. Relat. Mater. 97, 107426.

Ding, E.-X., Wang, J., Geng, H.-Z., et al, 2015. Y-junction carbon nanocoils: synthesis by chemical vapor deposition and formation mechanism. Sci. Rep. 5, 1–9.

Dursun, Z., Gelmez, B., 2010. Simultaneous determination of ascorbic acid, dopamine and uric acid at Pt nanoparticles decorated multiwall carbon nanotubes modified GCE. Electroanalysis: An International Journal Devoted to Fundamental and Practical Aspects of. Electroanalysis 22, 1106–1114.

Efimov, A., Laaksonen, T., 2022. The synthesis of palladium tetraarylphthalimidoporphyrin.

El-Nahass, M., Abu-Samaha, F., Menshawy, S., et al, 2014. Effect of annealing on structural and optical properties of copper tetraphenylporphyrin (CuTPP) thin films. Opt. Laser Technol. 64, 28–33.

Ensafi, A.A., Taei, M., Khayamian, T., 2009. A differential pulse voltammetric method for simultaneous determination of ascorbic acid, dopamine, and uric acid using poly (3-(5-chloro-2-hydroxyphenylazo)-4, 5-dihydroxynaphthalene-2, 7-disulfonic acid) film modified glassy carbon electrode. J. Electroanal. Chem. 633, 212–220.

Farajikhah, S., Innis, P.C., Paull, B., et al, 2019. Facile development of a fiber-based electrode for highly selective and sensitive detection of dopamine. ACS Sensors 4, 2599–2604.

Fathi, Z., Jahani, S., Zandi, M.S., et al, 2020. Synthesis of bifunctional cabbage flower–like Ho3 + /NiO nanostructures as a modifier for simultaneous determination of methotrexate and carbamazepine. Anal. Bioanal. Chem. 412, 1011–1024.

Foroughi, M.M., Noroozifar, M., Khorasani-Motlagh, M., 2015. Simultaneous determination of hydroquinone and catechol using a modified glassy carbon electrode by ruthenium red/carbon nanotube. J. Iran. Chem. Soc. 12, 1139–1147.

Foroughi, M.M., Jahani, S., Aramesh-Boroujeni, Z., et al, 2021a. Synthesis of 3D cubic of Eu3 + /Cu2O with clover-like faces nanostructures and their application as an electrochemical sensor for determination of antiretroviral drug nevirapine. Ceram. Int. 47, 19727–19736.

Foroughi, M.M., Jahani, S., Aramesh-Boroujeni, Z., et al, 2021b. Template-free synthesis of ZnO/Fe3O4/Carbon magnetic nanocomposite: Nanotubes with hexagonal cross sections and their electrocatalytic property for simultaneous determination of oxymorphone and heroin. Microchem. J. 170, 106679.

Giovannetti, R., 2012. The use of spectrophotometry UV-Vis for the study of porphyrins. Macro Nano Spectrosc., 87–108

Gnahore, G.T., Velasco-Torrijos, T., Colleran, J., 2017. The selective electrochemical detection of dopamine using a sulfated β-cyclodextrin carbon paste electrode. Electrocatalysis. 8, 459–471.

Guo, Y., He, D., Xie, A., et al, 2019. The electrochemical oxidation of hydroquinone and catechol through a novel poly-geminal dicationic ionic liquid (PGDIL)–TiO2 composite film electrode. Polymers. 11, 1907.

Huang, Q., Lin, X., Tong, L., et al, 2020. Graphene quantum dots/multiwalled carbon nanotubes composite-based electrochemical sensor for detecting dopamine release from living cells. ACS Sustainable Chem. Eng. 8, 1644–1650.

Huang, D.-L., Wang, J., Yuan, H.-Q., et al, 2018. Noncovalently copper-porphyrin functionalized reduced graphene oxide for sensitive electrochemical detection of dopamine. J. Porphyrins Phthalocyanines 22, 853–862.

Huang, Z., Zhang, L., Cao, P., et al, 2021. Electrochemical sensing of dopamine using a Ni-based metal-organic framework modified electrode. Ionics 27, 1339–1345.

Jandaghi, N., Jahani, S., Foroughi, M.M., et al, 2020. Cerium-doped flower-shaped ZnO nano-crystallites as a sensing component for simultaneous electrochemical determination of epirubicin and methotrexate. Microchim. Acta 187, 1–11.

Juska, V.B., Juska, G., 2021. Copper-nanostructure-modified laser-scribed electrodes based on graphitic carbon for electrochemical detection of dopamine and glucose. J. Chem. Technol. Biotechnol. 96, 1086–1095.

Karuppiah, C., Sakthinathan, S., Chen, S.M., et al, 2016. A non-covalent functionalization of copper tetraphenylporphyrin/chemi-

cally reduced graphene oxide nanocomposite for the selective determination of dopamine. Appl. Organomet. Chem. 30, 40–46.
Kausar, A., 2021. Polymer/carbon nanocoil nanocomposite: status and future directions. Polymer-Plast. Technol. Mater. 60, 816–829.
Kowalczuk, D., Pitucha, M., 2019. Application of FTIR method for the assessment of immobilization of active substances in the matrix of biomedical materials. Materials 12, 2972.
Kumar, S., Srivastva, A.N., 2021. Application of Carbon Nanomaterials Decorated Electrochemical Sensor for Analysis of Environmental Pollutants. Analytical Chemistry-Advancement, Perspectives and Applications, IntechOpen.
Lakard, S., Pavel, I.-A., Lakard, B., 2021. Electrochemical biosensing of dopamine neurotransmitter: A review. Biosensors. 11, 179.
Latif, S., Jahangeer, M., Razia, D.M., et al, 2021. Dopamine in Parkinson's disease. Clin. Chim. Acta 522, 114–126.
Li, Y.-Y., Kang, P., Wang, S.-Q., et al, 2021. Ag nanoparticles anchored onto porous CuO nanobelts for the ultrasensitive electrochemical detection of dopamine in human serum. Sens. Actuators, B 327, 128878.
Li, R., Yang, T., Li, Z., et al, 2017. Synthesis of palladium@ gold nanoalloys/nitrogen and sulphur-functionalized multiple graphene aerogel for electrochemical detection of dopamine. Anal. Chim. Acta 954, 43–51.
Lin, J.-H., Du, X.-S., 2021. Novel in situ growing carbon nanocoils onto steel mesh as positive electrode and hexagonal-MoO3 microrod array onto carbon fabric as negative electrode for assembling dual-asymmetric supercapacitors with redox active gel eleectrolyte. J. Power Sources 515, 230626.
Luhana, C., Moyo, I., Tshenkeng, K., et al, 2022. In-sera selectivity detection of catecholamine neurotransmitters using covalent composite of cobalt phthalocyanine and aminated graphene quantum dots. Microchem. J. 107605.
Lv, M., Mei, T., Wang, X., 2014. Selective and sensitive electrochemical detection of dopamine based on water-soluble porphyrin functionalized graphene nanocomposites. RSC Adv. 4, 9261–9270.
Nam, E., Derrick, J.S., Lee, S., et al, 2018. Regulatory activities of dopamine and its derivatives toward metal-free and metal-induced amyloid-β aggregation, oxidative stress, and inflammation in Alzheimer's disease. ACS Chem. Neurosci. 9, 2655–2666.
Neti, V.S.P.K., Wang, J., Deng, S., et al, 2015. Synthesis of a polyimide porous porphyrin polymer for selective CO2 capture. J. Chem.
Nia, N.A., Foroughi, M.M., Jahani, S., et al, 2019. Fabrication of a new electrochemical sensor for simultaneous determination of codeine and diclofenac using synergic effect of feather-type La3+-ZnO nano-flower. J. Electrochem. Soc. 166, B489.
Pakapongpan, S., Mensing, J.P., Phokharatkul, D., et al, 2014. Highly selective electrochemical sensor for ascorbic acid based on a novel hybrid graphene-copper phthalocyanine-polyaniline nanocomposites. Electrochim. Acta 133, 294–301.
Palakollu, V.N., Chiwunze, T.E., Liu, C., et al, 2020. Electrochemical sensitive determination of acetaminophen in pharmaceutical formulations at iron oxide/graphene composite modified electrode. Arabian J. Chem. 13, 4350–4357.
Pandikumar, A., How, G.T.S., See, T.P., et al, 2014. Graphene and its nanocomposite material based electrochemical sensor platform for dopamine. RSC Adv. 4, 63296–63323.
Peik-See, T., Pandikumar, A., Nay-Ming, H., et al, 2014. Simultaneous electrochemical detection of dopamine and ascorbic acid using an iron oxide/reduced graphene oxide modified glassy carbon electrode. Sensors 14, 15227–15243.
Phromsatit, T., Jantayot, W., Pinsuwan, K., et al., 2016. Thermal behavior and the solvent effects of ρ-Methoxy Tetraphenylporphyrin (TOMPP), Copper Porphyrin (CuTOMPP), and Nitroporphyrin (CuTOMPP-NO2). MATEC Web of Conferences, EDP Sciences.
Poudyal, D.C., Satpati, A., Kumar, S., et al, 2019. High sensitive determination of dopamine through catalytic oxidation and preconcentration over gold-multiwall carbon nanotubes composite modified electrode. Mater. Sci. Eng., C 103, 109788.
Reddy, A.L.M., Jafri, R.I., Jha, N., et al, 2011. Carbon nanocoils for multi-functional energy applications. J. Mater. Chem. 21, 16103–16107.
Sakthinathan, S., Lee, H.F., Chen, S.-M., et al, 2016. Electrocatalytic oxidation of dopamine based on non-covalent functionalization of manganese tetraphenylporphyrin/reduced graphene oxide nanocomposite. J. Colloid Interface Sci. 468, 120–127.
Senge, M.O., Sergeeva, N.N., Hale, K.J., 2021. Classic highlights in porphyrin and porphyrinoid total synthesis and biosynthesis. Chem. Soc. Rev. 50, 4730–4789.
Setoudeh, N., Jahani, S., Kazemipour, M., et al, 2020. Zeolitic imidazolate frameworks and cobalt-tannic acid nanocomposite modified carbon paste electrode for simultaneous determination of dopamine, uric acid, acetaminophen and tryptophan: Investigation of kinetic parameters of surface electrode and its analytical performance. J. Electroanal. Chem. 863, 114045.
Stoikov, I., Ageeva, M., Shamagsumova, R., et al, 2011. Dopamine Sensor Based on a Composite of Silver Nanoparticles Implemented in the Electroactive Matrix of Calixarenes. Electroanalysis 23 (10), 2281–2289.
Su, D., Pan, L., Fu, X., et al, 2015. Facile synthesis of CNC–MnO2 hybrid as a supercapacitor electrode. Appl. Surf. Sci. 324, 349–354.
Tavakolian-Ardakani, Z., Hosu, O., Cristea, C., et al, 2019. Latest trends in electrochemical sensors for neurotransmitters: A review. Sensors 19, 2037.
Vickers, N.J., 2017. Animal communication: when i'm calling you, will you answer too? Curr. Biol. 27, R713–R715.
Wu, L., Feng, L., Ren, J., et al, 2012. Electrochemical detection of dopamine using porphyrin-functionalized graphene. Biosens. Bioelectron. 34, 57–62.
Wu, J., Sun, Y.-M., Wu, Z., et al, 2019. Carbon nanocoil-based fast-response and flexible humidity sensor for multifunctional applications. ACS Appl. Mater. Interfaces 11, 4242–4251.
Yan, J., Liu, S., Zhang, Z., et al, 2013. Simultaneous electrochemical detection of ascorbic acid, dopamine and uric acid based on graphene anchored with Pd–Pt nanoparticles. Colloids Surf., B 111, 392–397.
Zaeri, M.M., Ziaei-Rad, S., 2015. Elastic behavior of carbon nanocoils: A molecular dynamics study. AIP Adv. 5, 117114.
Zhao, H.-X., Mu, H., Bai, Y.-H., et al, 2011. A rapid method for the determination of dopamine in porcine muscle by pre-column derivatization and HPLC with fluorescence detection. J. Pharm. Anal. 1, 208–212.
Zhu, Z., 2017. An overview of carbon nanotubes and graphene for biosensing applications. Nano-micro Lett. 9, 1–24.